Numerical Investigation of Gas Generator and Preburner Flows for Rocket Engine Applications

Björn Kniesner, Manuel Frey and Oliver Knab
Astrium GmbH Space Transportation
D-81663 München
bjoern.kniesner@astrium.eads.net, manuel.frey@astrium.eads.net, oliver.knab@astrium.eads.net

Abstract
For the layout and optimization of rocket combustion devices such as thrust chambers, gas generators and preburners Astrium applies the in-house code Rocflam-II, which is an axisymmetric Navier-Stokes solver with a Lagrange droplet tracking module. In the paper a H_2/O_2 preburner and a CH_4/O_2 gas generator flow are considered showing up several new computational aspects compared to thrust chamber flows such as low mixture ratio, small number of injection elements, transcritical cooling film, complex injection elements and additional mixing devices. As far as available, computational results are compared to experimental data.

1. Introduction

In the frame of an Astrium R&D activity as well as the national technology research program TEKAN 2010 II gas generator and preburner combustion devices were needed for testing purpose. For this reason Astrium started building up experience and knowledge within this technical domain – both on experimental as well as on computational side. The national program focused on a regeneratively cooled H_2/O_2 preburner in a staged combustion cycle subscale setup, which has been tested at several load points with a well equipped instrumentation. Within the Astrium R&D activity a film cooled CH_4/O_2 gas generator is being investigated. Here, first tests have been accomplished using a single injection element as preparation for follow-on fullscale tests to be performed in the future.

Gas generators and preburners mainly differ concerning two aspects. Gas generators are employed in open cycle (gas generator) engines in order to supply the turbines for driving the turbopumps using about 3 to 5% of the total engine mass flow. Preburners are used in closed cycle (staged combustion) engines for the same purpose providing a mass flow rate in the order of 15 to 20% (fuel rich) which then is reinjected into the main chamber for complete combustion. Since the turbine exhaust flow of gas generators is dumped, gas generators operate at similar pressure level when compared to main combustion chambers. In the case of preburners, however, the pressure level is much higher due to the staged combustion arrangement.

In contrast to main combustion chambers the primary aim of both gas generator and preburner development is not a highest possible performance but a uniform and sufficiently low temperature profile at the outlet to avoid problems for the downstream turbine. These differences imply several new computational aspects at the simulation of the considered gas generator and preburner compared to thrust chambers:

- Operation far from stoichiometric mixture ratio (mostly fuel rich mixture ratio compared to main combustion chamber ➔ also realized in the present case)
- Small number of injection elements ➔ modeling of 3D geometry in 2D simulation

In case of the CH_4 gas generator additional aspects have to be taken into account:

- Complex injection elements
- Very low fuel injection temperatures
- Transcritical CH_4 cooling film
- Additional mixing devices (i.e. turbulence ring)
- Possible soot appearance

2. Numerical Method

For the numerical investigation of the hotgas side of rocket combustion devices Astrium applies the in-house code Rocflam-II. Rocflam-II is an axisymmetric Navier-Stokes solver with a Lagrange droplet tracking module that incorporates several models for multi-class droplet tracking, evaporation and combustion, balancing their accuracy and computational effort. The turbulence modeling is realized via a two-layer k-ε model which switches to a one-equation model for the turbulent kinetic energy near the wall, determining the dissipation ε from an algebraic expression [1]. For the propellant combinations H_2/O_2 and CH_4/O_2 an equilibrium table-based chemistry model with a one-dimensional ppdf (presumed probability density function) approach taking into account the influence of turbulent combustion is used. No species concentration equations are solved, only a global mixture fraction and its variance are treated by differential equations.
The key of this type of combustion model is the combustion table which is computed separately prior to the computation itself by a chemical equilibrium code and a fluid database. A visualization of the chemistry tables for CH_4/O_2 and H_2/O_2 are given in Figure 1. Here the temperature evolution of the combustion between fuel and oxygen is shown as contour on the z-axis and additionally as contour color. On the other axis the gas solver input quantities mixture fraction f and enthalpy h are shown. Here, f=1 (O/F=0) means pure fuel, f=0 (O/F→∞) represents pure oxygen. The stoichiometric mixture of f≈0.2 (O/F≈4) for CH_4/O_2 and f≈0.112 (O/F≈8) for H_2/O_2 are indicated by the red arrows. The enthalpy level of zero corresponds to the injection temperature of fuel and oxidizer at f=1 and f=0 respectively. Positive enthalpy is related to higher, negative enthalpy is related to lower temperature. It is clearly visible that the combustion temperature increases with increasing enthalpy. At the stoichiometric ratio the temperature is maximal for the given enthalpy level. The tables are multi pressure tables which is necessary for a correct description of the flow and the combustion over the whole computational domain including throat and nozzle where the pressure strongly decreases. The effect of different pressure levels in the table (6 and 9 in the presented cases) is visible by the multiple contour layers. With increasing pressure dissociation becomes weaker resulting in a higher temperature at high pressure levels. In order to cope with the low mixture ratio (high mixture fraction) necessary for the gas generator simulation it was necessary to increase the number of levels below the stoichiometric ratio, otherwise oscillations occurred in the solution.
A further new aspect already addressed before is the low injection temperature of methane (≈110K). This actually necessitates the inclusion of low temperature data as well as additional species. The most important additional species would be liquid CO_2, liquid and solid H_2O but in principle, depending on the injection conditions, also solid CO_2 and liquid CO could occur. The extension of the table has up to now only been realized for liquid and solid H_2O - thus water and ice - in the frame of H_2/O_2 combustion. This effect is visible on the right side of Figure 1. At low enthalpy levels, which correlate with low temperature, the plateau in the two-phase region is visible. The liquid water, which exists in this region, is transported as additional species within the mixture thus forming a kind of dense-gas approach. The fluid properties of the liquid or solid phase are considered in the properties of the mixture. The introduction of low temperature data has considerable effect on the results, as was shown in [1]. Furthermore condensation effects within the flow as well as at the wall are captured.

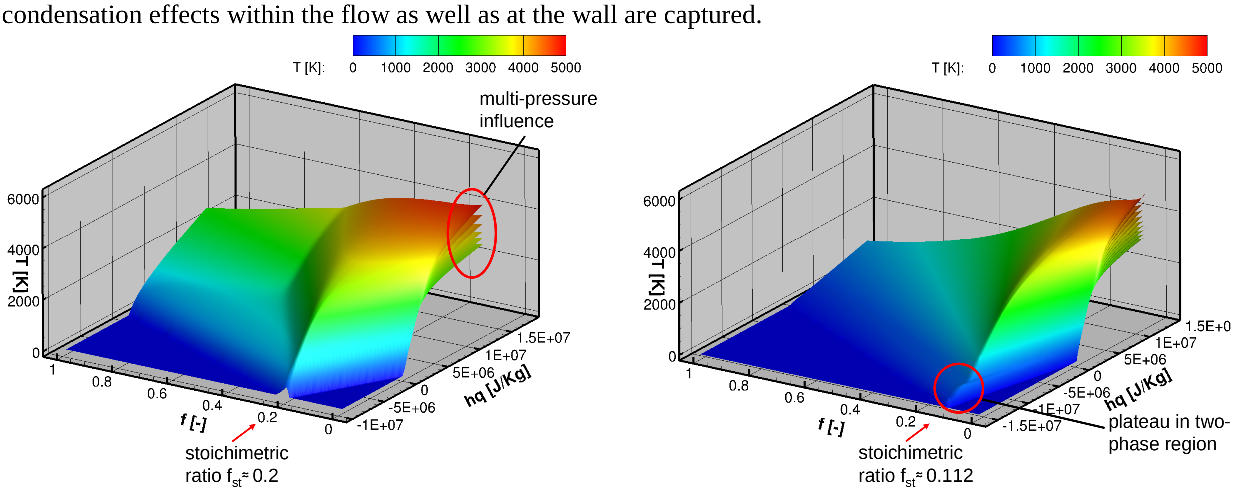

Figure 1: Multi-pressure equilibrium chemistry table for CH_4/O_2 (left) and H_2/O_2 combustion (right)

Considering the low mixture ratio below one for the gas generator application, soot may also play a role for CH_4/O_2 combustion. An analysis using a chemical equilibrium code shows an appearance of soot for mixture ratios lower than 1 of up to 14 % in mass fraction (Figure 2). However, during experiment this high soot mass fraction could not be observed. Similar observations have been reported in Russian and American publications concerning soot in methane combustion at low mixture ratios.

Another difference of the CH_4/O_2 combustion compared to H_2/O_2 is the coexistence of multiple reaction products – H_2O, CO_2 and CO – in the exhaust gas at low mixture ratio. The mixture ratio dependant balancing between these is responsible for the kink in the temperature profile around f=0.4 (O/F=1.5) at the left side of Figure 1 as well as in Figure 2. Important to note is that with suppression of soot in the equilibrium computation the temperature and the c*-curves in Figure 2 do not change significantly, meaning that from energetic point of view the occurrence or non-occurrence of soot does not significantly change the achievable temperature and performance level. For this reason soot is up to now neither considered in the chemistry table nor captured by extra modeling, nevertheless being aware that soot can have an influence onto the wall heat transfer when acting as kind of thermal barrier coating.

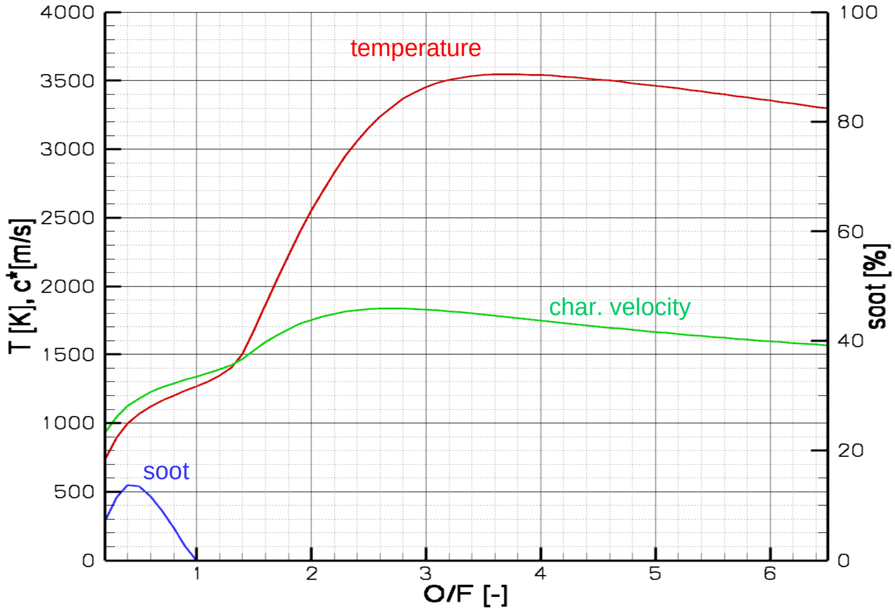

Figure 2: Occurrence of soot for CH_4/O_2 combustion at about 60 bar predicted by the chemical equilibrium Code

The axisymmetric code Rocflam-II is usually applied to 3D injection configurations. For the axisymmetric simulation, the single injection elements are transferred into injection rings as shown in Figure 3 for a subscale injection head with 19 coaxial elements. The injection of O_2 and CH_4 is realized via droplets in the Lagrange module, where the injection temperature, momentum and a droplet distribution are prescribed. Depending on the problem an order of magnitude of up to one million droplets are tracked throughout the combustion chamber, interacting with the gas phase and evaporating, which is modeled by source terms for mass, momentum and energy in the Navier-Stokes solver. This injection procedure allows prescribing the correct injection mass flow and velocity and thus the correct injection momentum although the simulated injection area is different.

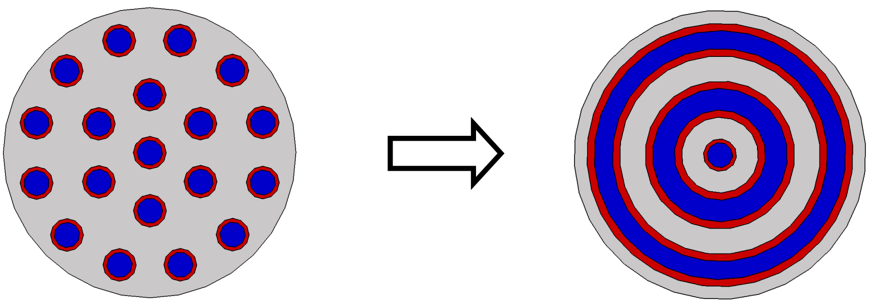

Figure 3: Sketch of an injection head with coaxial injection elements (left) and realization in the axisymmetric code Rocflam-II (right); red: fuel, blue: oxidizer

As soon as the number of injection elements is sufficiently high as it is normally the case for fullscale main combustion chambers (up to 500), the axisymmetric assumption is fairly appropriate. The ratio of the real area to the computationally assumed area is then close to one for fuel and around one third for oxidizer. For the 19 elements subscale injector head of Figure 3 which is mainly used for code as well as model validation and anchoring, the area ratios between implicitly modeled and real injection area are still comparable to the full scale main chamber values. The results obtained for this injector head show a very good agreement compared to experimental values except for the very first part of the chamber [2], [3] hence the error made by the axisymmetric assumption is judged to be small concerning wall heat flux, wall temperature and integral values such as combustion efficiency, thrust or specific impulse. For the presented gas generator as well as for the preburner only 7 injection elements are used. This decreases the area ratios for both fuel and oxidizer by a factor of 2 and consequently increases the error of the axisymmetric assumption.

The injection of the fluid as droplet in the Lagrange module is also applied for fluids of supercritical pressure at subcritical temperature (transcritical state), which is the case for oxygen in both presented applications and for methane in the gas generator (comp. Figure 4). The fact that in this thermodynamic state no surface tension and no latent heat of evaporation exist is considered and droplet tracking is ensured by a special treatment within the Lagrange module. However, the good agreement of the results for H_2/O_2 combustion [2] as well as CH_4/O_2 combustion [3] for main chamber mixture ratios, confirms that this kind of modeling is well suited even for transcritical state.

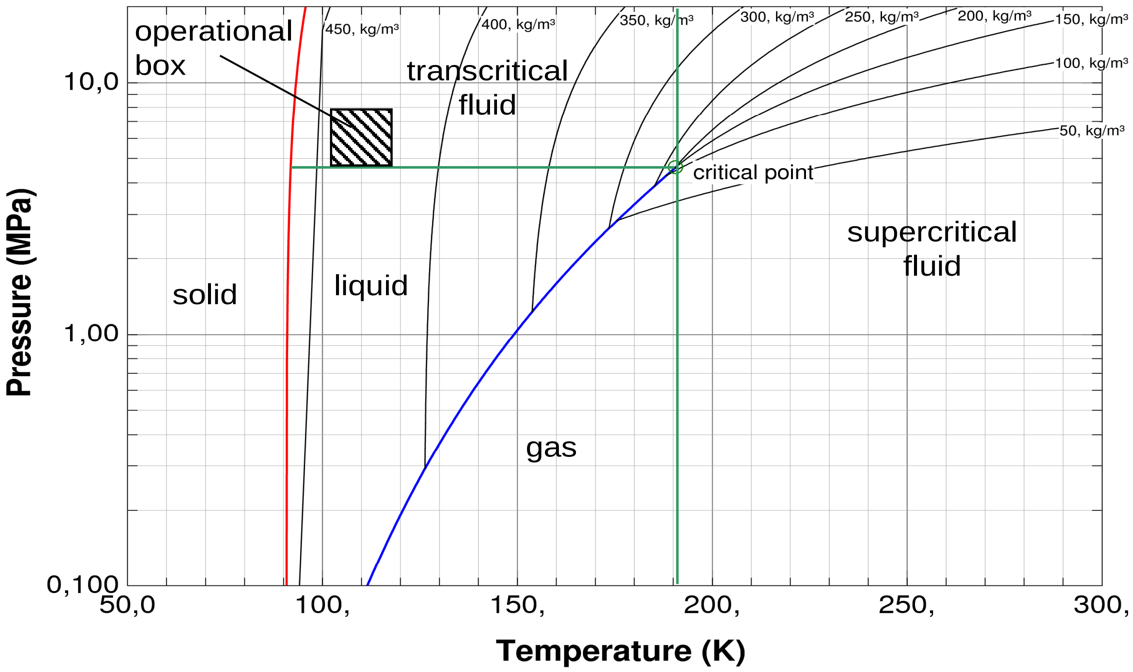

Figure 4: Phase diagram of methane including the thermodynamical injection state of the operational box

For the methane gas generator an additional CH_4 cooling film is intended. This film is treated in analogy to the core injection, thus by the transcritical injection through the Lagrange module. The methane then moves along the wall and builds up the film in the gas solver.

For the determination of the wall temperature the coolant side has to be modeled as well. In case of no active cooling as for the methane gas generator this is realized directly within Rocflam-II by solving a quasi two dimensional (radial and longitudinal) energy balance equation with radiation at the outer surface. For the preburner with a regenerative cooling Rocflam-II is loosely coupled to an empirical-correlation based in-house tool named RCFS-II [4].

3. H_2/O_2 Preburner

As already mentioned in the introduction a preburner is characterized by a relatively high mass flow and a high pressure level compared to a gas generator. The considered H_2/O_2 preburner has one central and six circularly arranged coaxial elements and operates at a mixture ratio of O/F=0.66 and chamber pressure levels increasing from 74 to 210 bar. Figure 5 shows a sketch of the experimental setup, including the injection positions. The chamber consists of four water cooled segments so that calorimetric measurements of the wall heat flux are possible. The first segment additionally is coated by a thermal barrier coating (TBC) which is accounted for on the coolant side computation mainly. Its influence for the Rocflam-II computation is accounted for by an increased surface roughness and a higher wall temperature as result of the coupling in this area. For the rest of the chamber measured surface roughness values have been implemented. The four segments are followed by a tube segment with an orifice as throat in order to create a sonic outflow.

Concerning the computational grid the wall normal distribution respects the need of the low-Re turbulence model to properly resolve the boundary layer by dimensionless wall distance values of y^+ ranging from 0.3 to 0.8 along the chamber wall. On the symmetry axis values of $\Delta y^+ \approx 1000$ are reached. In axial direction values ranging from $\Delta x^+ \approx$ 1000 to 5000 are chosen. All grid expansion or compression factors are realized below 10%.

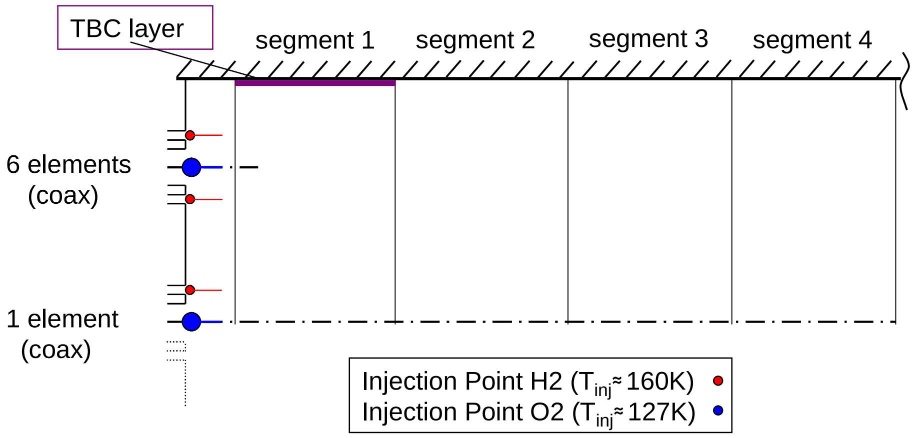

Figure 5: Sketch of the experimental preburner setup, including injection positions and caloric segments (throat segment follows downstream – not shown here)

In Figure 6 the comparison of the computed wall heat flux profile and the calorimetrically measured wall heat load is depicted for a mixture ratio of O/F=0.66 and chamber pressure levels increasing from 74 to 210 bar. In the first segment the isolating influence of the TBC-layer is clearly visible. In the second segment the wall heat flux is maximal, decreasing slightly moving downstream. The kind of saw-tooth profile is due to the consideration of an inflow effect into the channel on the coolant side computation, which additionally decreases the wall temperature in the first part of the cooling channel. The resulting strong wall heat flux response is due to the low combustion temperature compared to main combustion chambers where the wall heat flux is less sensitive to a wall temperature increase. In general it is visible that the wall heat flux in experiment decreases significantly stronger than in the simulation when moving downstream so that the heat flux in the last segment is strongly over-predicted. This could be due to an insufficiently strong predicted recirculation zone upstream of the severe contour change at the beginning of the throat segment. For the first two segments the agreement is quite good in terms of absolute wall heat flux level as well as relative difference between the different pressure levels, especially keeping in mind that the measurement scattering is also quite elevated.

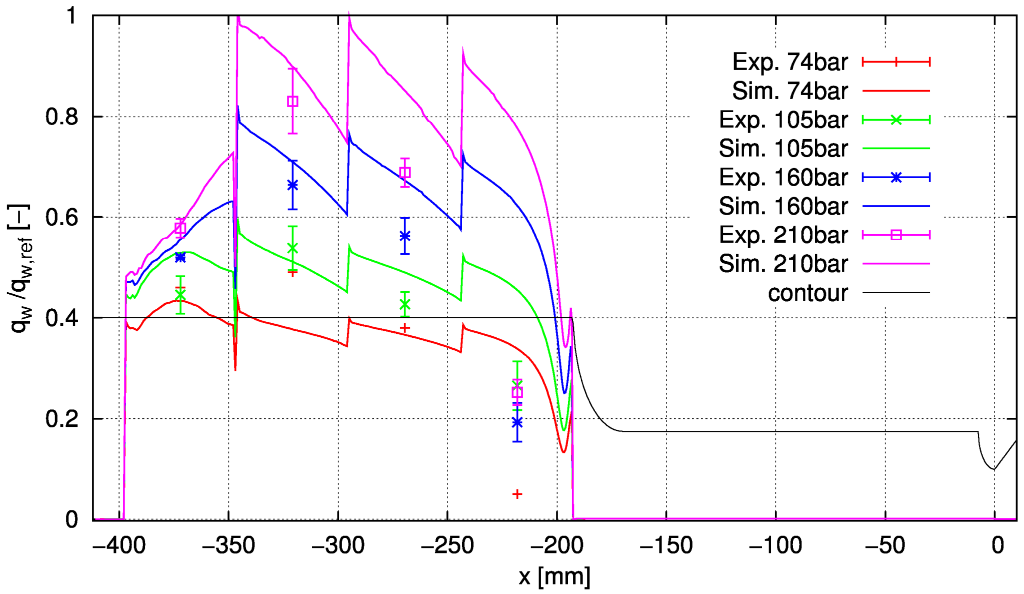

Figure 6: Comparison of wall heat flux prediction and preliminary caloric measurement of the H_2/O_2 preburner at a mixture ratio of O/F= 0.66 and chamber pressure levels increasing from 74 to 210 bar

In the upper left part of Figure 7 a contour plot of temperature (upper half) and mixture ratio (lower half) is depicted. As the part of the geometry downstream of x=-200 mm including the two contractions has only been added for testing purpose, the investigation concentrates on the first cylindrical section (x<-200mm). It is visible that locally in the region of the injection elements the mixture ratio and thus also the temperature are quite high, reaching up to 1600K. However, mixing in the chamber works well – supported by the big recirculation zone between the injection elements – so that the temperature appears quite uniform already after approximately 40% of the cylinder length.

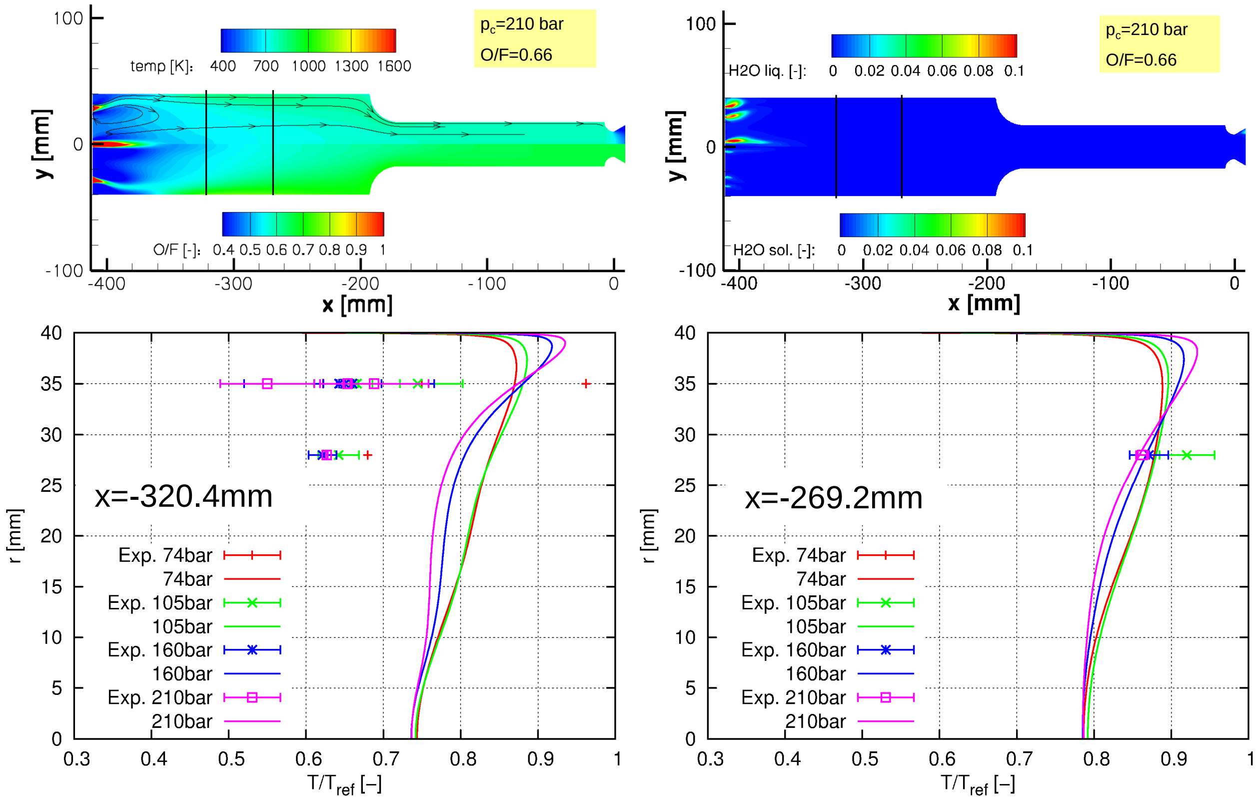

Figure 7: Contour plots of temperature and mixture ratio (upper left) as well as mass fraction of liquid and ice (upper right) with radial temperature profiles at two different axial locations of several simulations of the H_2/O_2 preburner at a mixture ratio of O/F= 0.66 and pressure levels increasing from 74 to 210 bar

In the upper right part of Figure 7 the influence of the low temperature data in the combustion table is visualized. In the injection area a substantial mass fraction of liquid water (upper part) and even ice (lower part) can be observed. Very close to the wall and thus not visible in the Figure a perceptible amount of condensed liquid water is predicted, also contributing to the wall heat flux.

Looking more in detail at the first available axial measurement position (Figure 7 bottom left) reveals that at this location the temperature level is predicted too high compared to the preliminary experimental temperature measurements which are available at 60 and 80% of the chamber radius. The general trend of the temperature at the lower pressure level being lower than at the high pressure levels up to r=35mm is nevertheless predicted correctly. At the second axial location situated at around 60% of the cylinder length the agreement is very good concerning both absolute temperature level and relative temperature difference for varying pressure level. Considering both observations it seems that either evaporation or mixing is predicted to occur faster than in the experiment.

4. CH_4/O_2 Gas Generator

In contrast to the H_2/O_2 preburner the CH_4/O_2 gas generator is operated at significantly lower pressure. As can be deduced from Figure 4 the operational chamber pressure ranges around 50 bar. The mixture ratio is situated around 0.4. As this concept does not provide a regenerative cooling, a fuel film at the chamber wall is foreseen. As already discussed in Chapter 2 this transcritical film is modeled in analogy to the transcritical droplet injection. Comparable to the preburner the fullscale injector head has seven elements – one central and six circularly arranged. However, first element screening tests have been conducted with a subscale hardware consisting of the single central element only. The outer wall is placed where the circularly arranged elements are situated in the fullscale hardware. In contrast to the preburner the injection elements are not coax type but a combination of a double swirl and an impinger element. Details concerning the computational realization of the injection can be seen in Figure 8 where the geometry of the single-element subscale chamber for which test data are available is illustrated.

The double swirl core of the element is taken into account by different initial angles of the droplet trajectories for methane and oxygen depending on the element layout. The fuel jets that penetrate the double swirl cone enter the chamber at zero angles.

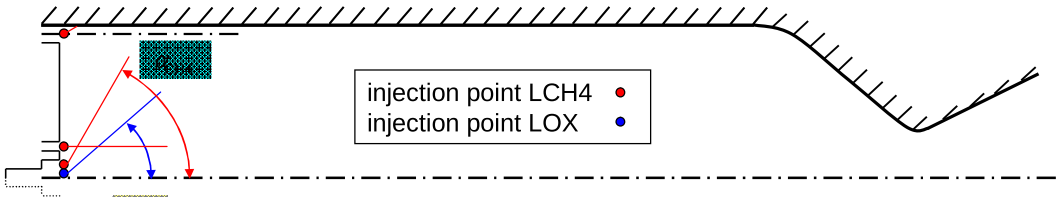

Figure 8: Geometry of the single-element subscale CH_4/O_2 gas generator with scheme of the injection head and indication of the injection positions for methane and oxygen

However, the penetration is not modeled in terms of droplet collision, but implicitly reflected by the choice of the droplet diameter spectrum. The film injector is situated very close two the wall at about 1mm below the chamber wall. In reality the film is injected with a circumferential swirl. Of course, in the frame of a two dimensional description this swirl can not be captured. The swirl mainly ensures that the liquid film is closed around the circumference which in the axisymmetric computation is satisfied per definition. Finally, for the film injection only the real axial velocity component is considered so that the axial momentum is correctly represented.
Another difference compared to the preburner is the additional mixing device. For full- and subscale two variants – a simple turbulence ring and a more complex turbulence grid – are envisaged. So far only the simple turbulence ring has been used in test. Simulation results suggest that the ring does not change the results significantly. Due to the three-dimensionality of the turbulence grid its consideration in the axisymmetric computation is difficult and has up to now not been solved. Experimental evidence of this phenomenon is not available yet but will be provided in the future.

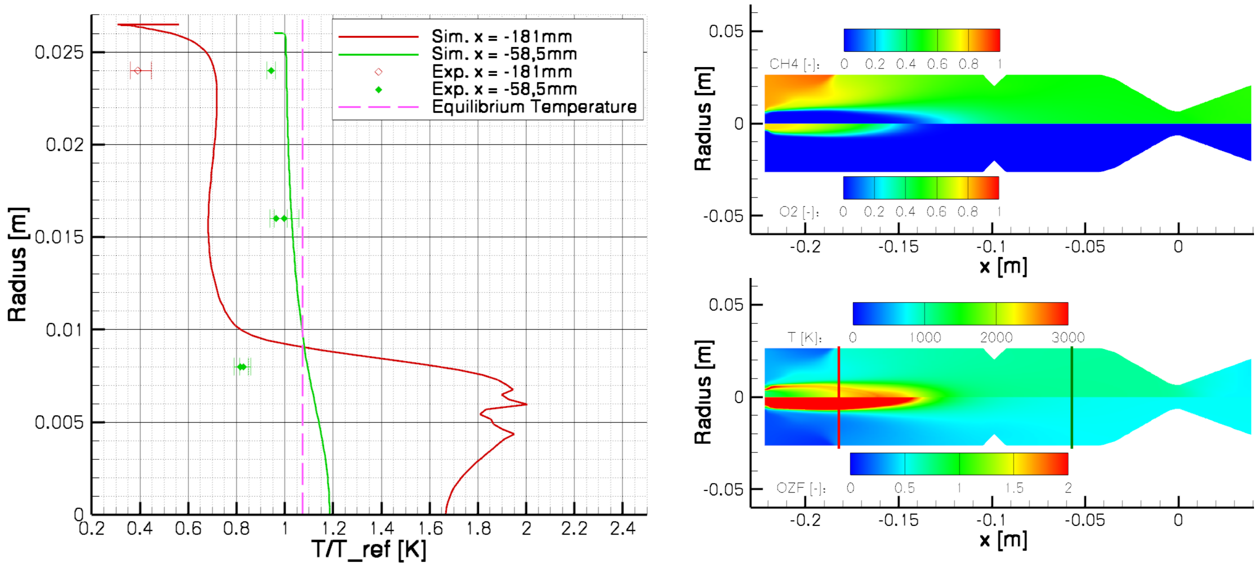

Figure 9: Computational and experimental radial temperature evolution of the CH_4/O_2 single-element subscale gas generator at two different axial locations (left) and contour plots of fuel and oxidizer mass fraction (upper right) as well as temperature and mixture ratio (lower left)

Concerning the computational grid the resolution of the full- as well as the subscale case resemble the one of the preburner. The wall normal distribution resolves the boundary layer by dimensionless wall distance values of y^+ ranging from 0.5 to 0.9 along the chamber wall. On the symmetry axis values of $\Delta y^+ \approx 1000$ are reached. In axial direction values vary between $\Delta x^+ \approx 1000$ and 5000. All grid expansion or compression factors are realized below 10%.
Figure 9 presents the results of the CH_4/O_2 single-element subscale gas generator. In the lower right part of the Figure contour plots of temperature and mixture ratio are shown. In the left part radial temperature profiles at selected locations have been extracted for comparison with experimental data. It turns out that at the backmost location (green, ≈90% of the cylinder length) the profiles are very uniform and thus fuel and oxidizer are nearly completely mixed. The temperature level furthermore matches quite well to the equilibrium calculation, indicating high combustion efficiency. At the front location (red) regrettably only one reliable measurement is available, showing a relatively low temperature and thus good film effectiveness in this region. In the computation the strong film cooling effect vanishes just shortly upstream of this front location as can be deduced best from the contour plot on the upper right of the Figure where the fuel mass fraction suddenly decreases substantially. This decrease is directly translated into a mixture ratio increase leading to a substantially higher temperature (lower right side) and

thus overprediction compared to experiment. The location where the film effect vanishes is strongly affected by the recirculation zone which in turn is driven by the effective exit angle and velocity of the element. Consequently the element exit properties used in the computation need to be adjusted in order to predict a more realistic temperature profile at the front location. Judging from the computation, concerning uniformity of the temperature the turbulence ring does not seem to be necessary. Already upstream the ring location the temperature profile is quite uniform over the radius.

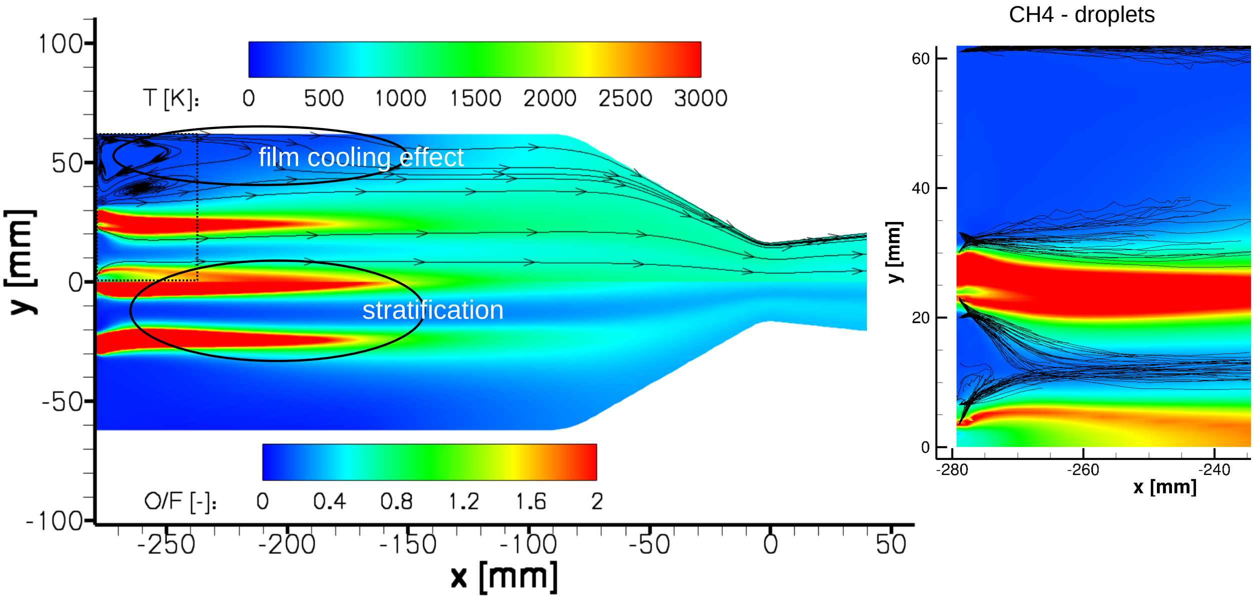

Figure 10: Temperature and mixture ratio contour plot (left) as well as visualization of the methane droplet trajectories in temperature zoom for the full scale gas generator in reference point

In Figure 10 the application of the modeling to the fullscale geometry with 6+1 elements is shown. In the upper half of the contour plot the temperature is presented, in the lower part the mixture ratio O/F. First of all the film cooling effect is clearly visible by the cold region near the outer wall. In the mixture ratio plot this corresponds well to the low, thus fuel rich region. Compared to the single element subscale computation (Figure 9) the film cooling effect is considerably stronger. This is linked to the considerably larger recirculation zone between the elements of the outer row and the wall compared to the central element and the wall in subscale, which is mainly due to a pushing downward of the outer row jets. This is possible because in contrast to the subscale configuration the outer row is some distance away from the symmetry axis of the device. However, considering the small number of elements it is questionable if this kind of circumferentially closed recirculation zone will be present in the real three-dimensional case. This indicates that in the fullscale case the mapping of 3D geometry to 2D simulation is questionable. Further investigations concerning this aspect are foreseen.

In order to give a hint of the Euler/Lagrange interaction, on the right side of Figure 10 the methane droplet trajectories are visualized. In the background the temperature is shown. The differently prescribed initial angles are clearly visible. After some distance the droplets are entrained by the gas flow and deflected in streamwise direction. The film injector droplets remain close to the wall and form the fuel rich film layer.

Concerning the central element its temperature and mixture ratio behavior strongly resembles the subscale result. Nevertheless, the hot core which is mainly due to the relatively high local mixture ratio of the elements reaches farer into the chamber than in the subscale case. This also hinders the quick temperature decrease further downstream by mixing with the cool outer flow and leads to a perceptible amount of temperature inhomogenity at the end of the cylindrical section. This is reflected in Figure 11 left where the temperature averaged in radial direction as well as the unmixedness are shown in order to give a hint concerning the degree of mixing in the gas generator. The unmixedness depicts a radially averaged quantity. Its value of 1 represents a completely unmixed composition whereas a value of 0 corresponds to a perfect mixture. At the end of the cylinder the value of the unmixedness remains around 0.2 which would lead to a certain loss in performance. However, one has to keep in mind that the additional turbulence grid, also foreseen for the fullscale application, has up to now not been taken into account. The evolution of the averaged temperature corresponds well to the one of the unmixedness. The better the mixture becomes, the more temperature approaches the theoretically possible limit.

On the right side of Figure 11 the wall temperature distribution for the reference as well as a high load point is shown. As expected the maximal wall temperature little upstream of the throat is highest for the high load point, linked to the shortest film length. For both load points the cooling effect of the transcritical film is nicely reproduced and even looks comparable to simulations of other film cooled engines with liquid films.

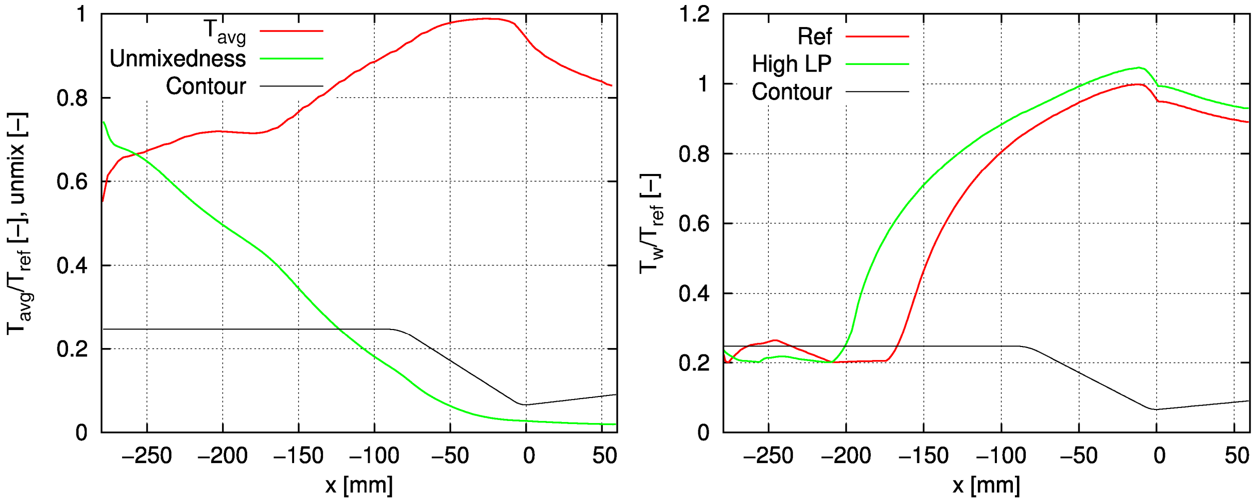

Figure 11: Axial evolution of unmixedness and averaged temperature (left) as well as axial wall temperature evolution at different load points (right) for the fullscale CH_4/O_2 gas generator without turbulence ring at a global mixture ratio of about O/F=0.4 and pressure around 50bar

5. Summary and Conclusion

The numerical investigation of the flow in a H_2/O_2 preburner and a CH_4/O_2 gas generator has been accomplished successfully especially concerning five of the new aspects being mentioned at the beginning.
The low mixture ratio compared to main combustion chambers posed no further problems when properly adapting the combustion tables. The transcritical CH_4 cooling film was realized in analogy to the core fuel injection as transcritical fluid which resulted in a realistic wall temperature distribution and a good agreement with test data. The complex injection elements have been modeled by several injection positions at different angles according to the element layout, which results in a realistic flow field. The additional mixing ring present in the CH_4/O_2 gas generator single element test was modeled. Its effect in the computation is quite small. However, a stronger effect is expected by the turbulence grid, which has not been tested up to now and whose inclusion in the axisymmetric simulation will be complicated. A possible soot appearance was investigated by consulting a chemical equilibrium code, own test data as well as available open literature and it appears that neglecting soot for CH_4/O_2 combustion at mixture ratios around 0.4 can be justified.
Concerning the two remaining points, 2D ⇔ 3D modeling and CO_2 low temperature data, investigations and actions already started but have up to now not been completed.
The error made by mapping of the 3D geometry to a 2D axisymmetric simulation, which is strongly affected by the small number of injection elements, is up to now difficult to judge as no 3D simulation tool with comparable features is available at the moment. It turned out that especially with a small number of elements the position and size of the recirculation zone, which strongly affects the global mixing and thus temperature as well as heat flux distribution, is very sensitive to the parameters of the injection.
The inclusion of the low temperature data of CO_2 which is necessary due to the very low CH_4 injection temperature is currently work in progress.
The obtained results show that the current modeling status already produces reasonable results concerning mixing efficiency, wall temperature and film effectiveness. Hence, the applicability of Rocflam-II to gas generator and preburner problems has been demonstrated and will be used to support the further development.

Acknowledgements

Part of this work was performed within the national technology program TEKAN 2010 II. This program is sponsored by the German Space Agency, DLR Bonn, under contract No. 50RL0710.

References

[1] W. Rodi: "Experience with 2-layer models combining the k-ε model with a one-equation model at the wall", AIAA-91-0216, 29th Aerospace Sciences Meeting, Reno, Nevada, 1991
[2] M. Frey, B. Kniesner and O. Knab: "Consideration Of Real Gas Effects And Condensation In A Spray Combustion Rocket Thrust Chamber Design Tool ", EUCASS2009-85, 3rd European Conference for Aerospace Sciences (EUCASS), Versailles, France, 2009
[3] J. Görgen, T. Aichner and M. Frey: "Spray Combustion and Heat Transfer Modelling in LOX/H2, LOX/HC and MMH/NTO Combustion Chambers", EUCASS2009-104, 3rd European Conference for Aerospace Sciences (EUCASS), Versailles, France, 2009
[4] C. Mäding, D. Wiedmann, K. Quering and O. Knab: "Improved Heat Transfer Prediction Engineering Capabilities for Rocket thrust Chamber Layout", EUCASS2009-90, 3rd European Conference for Aerospace Sciences (EUCASS), Versailles, France, 2009